International Society for Rock Mechanics and Rock Engineering
Macedonian Association for Geotechnics

ISRM Regional Symposium
Eurock 2026
Risk Management in Rock Engineering
Skopje, 15-19 September

DOI: https://doi.org/10.68732/2f2a6c4f050c932b

ISBN: 978-9989-2053-6-1

Tensile fracturing in granite and gneiss investigated by DIC and thin sections

L. Jacobsson & M. Flansbjer
Department of Chemistry and Applied Mechanics, RISE Research Institutes of Sweden, Borås
lars.jacobsson@ri.se
0000-0003-4526-4061

L. Brander
Raw Material Supply, Swerock AB, Göteborg, Sweden

J. Sandström
Surface Ships, Saab Naval, Karlskrona, Sweden

Abstract

The fracture mechanics properties in crystalline rocks depend on the microstructure, and presence of microcracks and pores. The aim was to visualize and quantify tensile fracturing properties during and after experiments. Wedge splitting tests were conducted on two quasi-brittle rock types, a medium- to coarse-grained granite and a finely medium-grained gneiss, to study the fracture processes and to determine fracture mechanics data under tensile loading. The propagating crack was followed during loading by displacement field measurements obtained from digital image correlation analysis. The propagating crack was meandering and branching in the granite, whereas the crack was straighter and smoother with almost no branching in the gneiss. The crack opening displacement was determined from the displacement field in a small band enclosing the crack path and was used to determine fracture process zone data. A fully developed crack, i.e. no cohesive force, was obtained when the crack opening displacement was about 6.5–20 μm in the granite and ≤ 6.5 μm in the gneiss. The length of the process zone was 10 mm initially and increasing to 15 mm when the crack length was 30–40 mm in the granite and 2–3 mm in the gneiss. The results on granite are in line with the few existing results in literature, whereas no previous results on gneiss were found. The onset of crack initiation was determined by the change of the crack mouth opening stiffness and compared with crack opening displacements yielding the same result. The thin section analyses confirmed mentioned observations on the crack path and showed occasionally several parallel crack paths in the granite, but a single crack path in the gneiss with a small amplitude and long wavelength. Intragranular fractures are mainly found in feldspar and large quartz grains. Several of the used methods are novel.

Keywords

Wedge splitting test, Crystalline rock, Mode I fracture mechanics, Fracture process zone (FPZ), Digital image correlation (DIC).

1 Introduction

The fracture mechanics properties in crystalline rocks depend on its mineral composition and microstructure, such as grain size, grain shape, shape and crystallographic orientation, and presence of microcracks and pores. Considering fracturing under tensile loading, many of the cracks pass along grain boundaries. Some pass also through the grains, e.g. feldspars or biotite, if the crystallographic direction is favourable and the grain size large enough (Krantz 1983, Brander et al. 2014). Moreover, occasionally crack branching occurs (Kobayashi and Fourney 1978).

The conceptual model of the progressive tensile fracturing of a rock can be described by three stages visualized by a case when a notched specimen is subjected to a force yielding a tensile stress in the notch (Fig. 1a). Elastic deformations and occasional crack initiation take place in the notch area during stage 1. In stage 2, there will be systematic crack initiation in a zone surrounding the notch when the force is further increased. Finally in stage 3, a fully developed crack has formed and started to propagate with no remaining cohesive force in its tail. By looking at the crack opening displacement (COD) along a crack with length a, there are cohesive forces in the fracture process zone (FPZ) which vanishes when COD reaches COD_{cr} and are zero above this value (Barenblatt 1959). The effect of the cohesive force can be seen if the COD along the crack extension is studied and length of the FPZ (L_{FPZ}) can be determined (Fig. 1b).There are few studies where the FPZ in crystalline rock was studied e.g. Kobayashi and Fourney (1978), Labuz et al. (1985, 1987) and Maji and Wang (1992).

The fracture mechanics properties in a rock are often described by the fracture toughness K_{Ic} using linear elastic fracture mechanics (LEFM) and determined by standard tests. There have been questions raised about the suitability to use LEFM and standard fracture mechanics tests on rock due to the non-linear nature of the response of rocks and small ligament lengths in the standard tests which both violate the foundations in LEFM (e.g. Zhu and Joyce 2012). LEFM is widely used due to its experimental simplicity as compared to using non-linear fracture mechanics.

This paper focusses on the fracture process, i.e. initiation and propagation, in one granite and one gneiss. The aim is to visualize and quantify tensile fracturing properties during and after experiments using different methods. A full description of the study was reported by Jacobsson et al (2025) and Jacobsson and Brander (2025).The figures, some modified, are obtained from these publications.

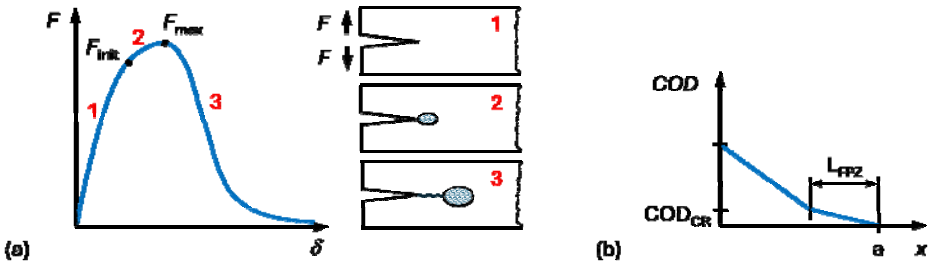


Fig. 1 (a) Example figure showing force versus displacement and stages during tensile fracturing: (1) occasional crack initiation, (2) systematic crack initiation with a partially developed FPZ, and (3) fully developed FPZ and crack propagation; (b) Crack opening displacement along the crack.

2 Experiments

One structurally isotropic medium- to coarse-grained igneous granite and one structurally anisotropic migmatitic and recrystallized orthogneiss were selected for this study. The gneiss consisted of parallel foliation layers of a finely medium-grained mesosome (70%–90% of the rock) and a medium- to coarse-grained leucosome. Petrographic characterizations and uniaxial compression, Brazilian, flexural strength and rupture energy tests were conducted to determine mechanical properties. Wedge Splitting Tests (WST), cf. Brühwiler and Wittmann (1990), were conducted to determine the fracture mechanics properties. The WST specimens are blocks with the dimensions 200 mm × 200 mm × 150 mm (height × width × thickness) manufactured with two types of notch geometries: either a "blunt" notch in shape of a borehole, or a sawn square-shaped notch (Fig. 2a). A constant rate of the crack mouth opening displacement,$CMOD$, of 15 µm/min was applied and the splitting force F_{s} was measured. The granite was tested with a sharp (GR-N) and blunt (GR-H) notch. The gneiss specimens (GN-A, GN-B and GN-C) had a blunt notch and were split in three directions A, B and C to study the effect of anisotropy (Fig 2b). Three specimens of each type were tested, i.e. 15 specimens in total.

The displacement field was measured on one face on the specimen covering the area of the propagating crack using Digital Image Correlation (DIC), cf. Sutton et al. (2009). Two CCD cameras with 2048 × 2048 pixels resolution and 50 mm lens were used to capture the images on the specimen surface. The calibrated measurement volume was ca. 100 mm × 100 mm × 80 mm (Fig. 2a). The COD was measured along the main crack perpendicular to it over a 3 mm wide band surrounding the main crack path. Thin sections were made from the wedge-split blocks after testing, covering the entire length of fractures. The blocks were impregnated by fluorescent epoxy before and during the cutting operations. By this, fractures, microcracks, and other cavities were enhanced.

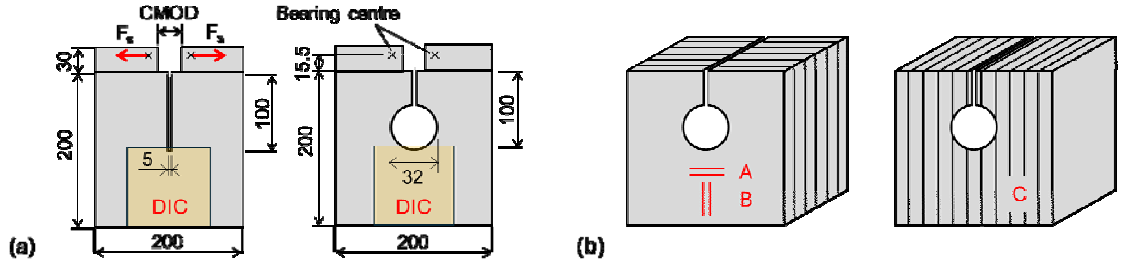


Fig. 2 (a) Specimen dimensions (mm), F_s , $CMOD$ and area for DIC measurements; (b) Black lines show the foliation planes for the gneiss. The red lines with labels A and B show the lineation directions. Label C shows splitting parallel to foliation.

3 Results

The splitting force $F_s$and the crack mouth opening stiffness $K_{\mathrm{CMOD}} = \mathrm{d}F_s/\mathrm{d}CMOD$ are shown in Fig. 3 and 4. A non-linearity at the loading phase and the relative ductility of the granite with a gradual force decrease at the post-peak part of the curve are seen in Fig. 3. The gneiss displays minor non-linearity at the loading part and its brittleness is seen by the rapid transition and load drop at the peak

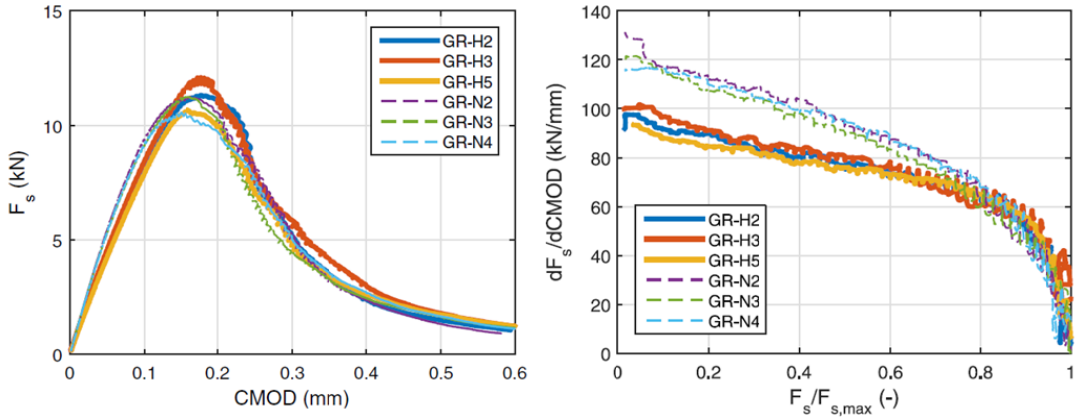


Fig. 3Left: Splitting force versus CMOD on granite specimens; Right: K_{CMOD} versus $F_s/F_{s,\max}$ up to peak load.

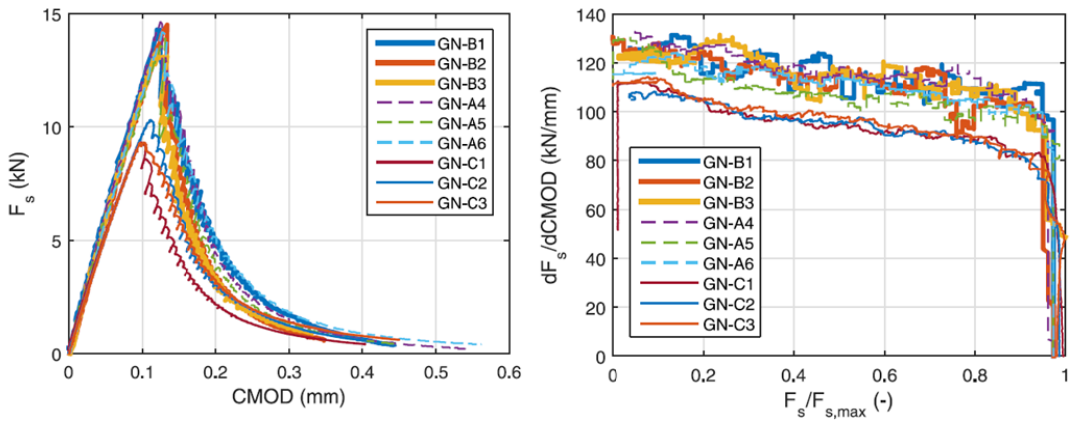


Fig. 4 Left: Splitting force versus CMOD on gneiss specimens; Right: K_{CMOD} versus $F_s/F_{s,\max}$ up to peak load.

load (Fig. 4). The onset of systematic crack initiation (stage 2 in Fig. 1) can be identified when the K_{CMOD}-curves change its slopes. For the granite, it appears to be approximately at $F_s/F_{s,\max}$ equal to 0.78±0.01 for the notched specimens and 0.90±0.02 for the specimens with the blunt notch when all specimens in the respective series are considered. The corresponding numbers for gneiss are 0.92±0.01 (type A and B) and 0.94±0.01 (type C).

The progressive fracturing in three specimens is visualized in Fig. 5–7. The propagating crack is meandering and branching in the granite (Fig. 5), whereas the crack is straighter and smoother with almost no branching in the gneiss (Fig.6 and 7). The onset for crack initiation was determined by the DIC measurements and was equal to the assessment based on changes in K_{CMOD}.

The COD value at full crack initiation,COD_{cr}, is between 10 and 20 µm on GR-H2. The gneiss specimens have a smaller COD_{cr}, ≤ 6.5 µm (GN-B1) and ≤ 4.4 µm (GN-C1).The length of the process zone (L_{FPZ}) was approximately 10 mm initially and increasing to 15 mm when the crack length was 30–40 mm in the granite (concluded by also comparing results on one more granite specimen not shown here) and 2–3 mm in the gneiss.

Looking further at the COD-results, the slope of the COD versus position x from the notch, i.e. the angle between the crack surfaces outside the FPZ begin to increase at a critical crack length (a = 55–60 mm) that was about the same on all specimens. The two observed phases correspond to (1) steady-state propagation without influence from bottom uncracked part of the specimen (ligament) and

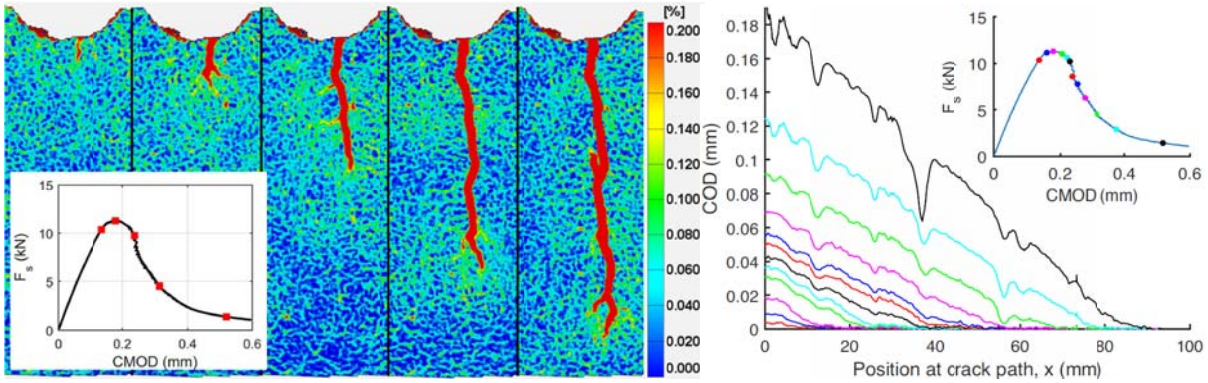


Fig. 5 Specimen GR-H2. Left: Largest principal strain at 5 load stages; Right: COD along the crack path at 12 load stages.

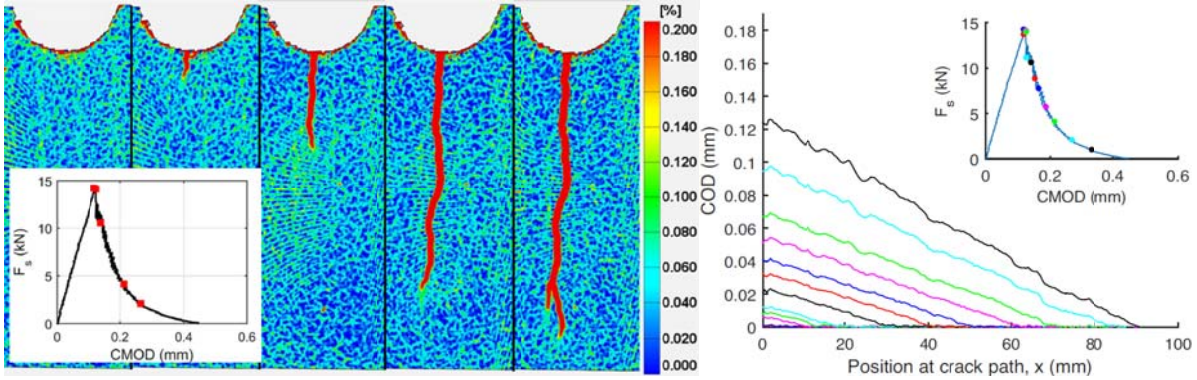


Fig. 6 Specimen GN-B1. Left: Largest principal strain at 5 load stages; Right: COD along the crack path at 12 load stages.

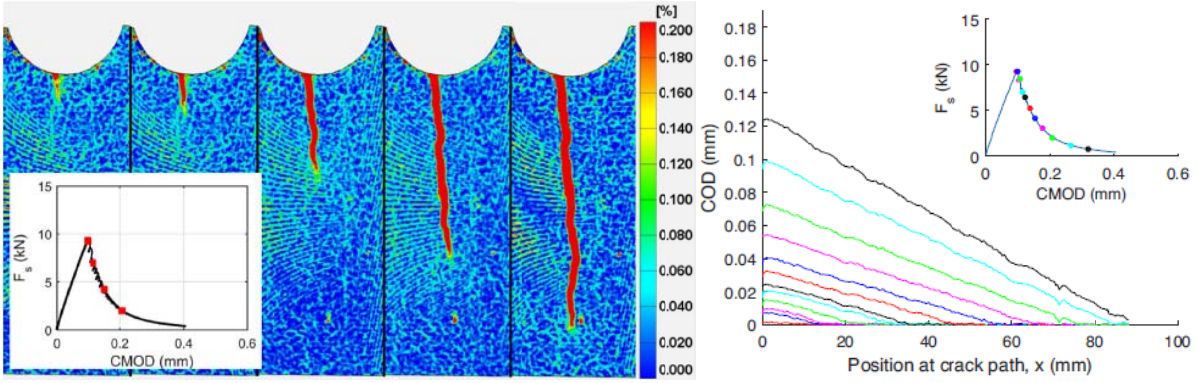


Fig. 7 Specimen GN-C1. Left: Largest principal strain at 5 load stages; Right: COD along the crack path at 12 load stages.

(2) propagation with influence from deformations in the ligament, cf. analogy with plastic hinge (Zhu and Joyce 2012). The deformation gradient becomes successively larger in the remaining part of the specimens that is uncracked with increasing crack length during phase (2). The deformation gradient affects the crack initiation and propagation (Zhu and Joyce 2012).

It is illustrative to study how the crack front advances with increased $CMOD$ to interpret the differences in ductility/brittleness (Fig. 8). There, the long crack initiation phase in the granite (GR-H2) and the instant and unstable propagation during the first 10–15 mm crack propagation in the gneiss (GN-B1 and GN-C1)can be seen. The position of the crack front a was determined at a COD-value of 2 and 4 µm.

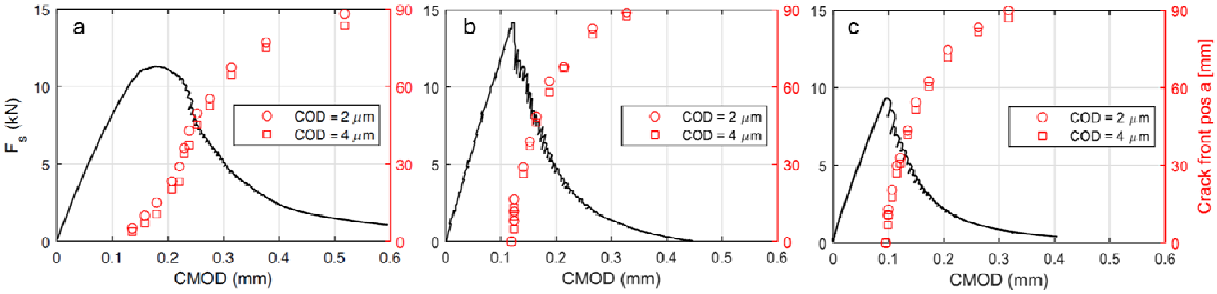


Fig. 8 Crack front position a and splitting force F_S versus $CMOD$ in specimen GR-H2 (a), GN-B1 (b) and GN-C1 (c).

The fracture energy and the strain energy release rate, G_{Ic}, were calculated using the WST-data (Fig. 3 and 4). The results showed that the granite required a much larger fracture energy to split than the gneiss. On the contrary, the maximum splitting force at the WST tests and tensile strength determined from the Brazilian and flexural strength tests were lower for the granite as compared with gneiss when the fractures were inflicted perpendicular to the foliation. This illustrates the difference in strength versus fracturing behaviour. The fracture toughness, K_{Ic}, was calculated from G_{Ic} and elasticity parameters determined from uniaxial compression tests yielding a larger value of K_{Ic} for the granite than for the gneiss. By analysing the test results using LEFM, it yielded consequently lower values of K_{Ic} as compared with values determined using non-linear fracture mechanics based on fracture energy. Moreover, the calculated K_{Ic} based on LEFM was larger in the gneiss when the blocks were split perpendicular to the than foliation, which is contrary to the results obtained from non-linear fracture mechanics. Several of the specimens had a blunt notch which violate the LEFM assumptions, but a relative comparison between the granite and gneiss should still hold.

A thin section image of one of the granite specimens is shown in Fig. 9a and illustrates the crack branching, parallel fractures and a high frequency of intragranular cracks in large grains. Similar branching was repeatedly seen along the main crack paths. A thin section image on one of the gneiss specimens, split perpendicular to the foliation (Fig. 9b), displays no crack branching and fewer intragranular cracks in the more fine-grained microstructure. Almost only grain boundary cracks are seen in Fig. 9c on a gneiss specimen split along the foliation planes.

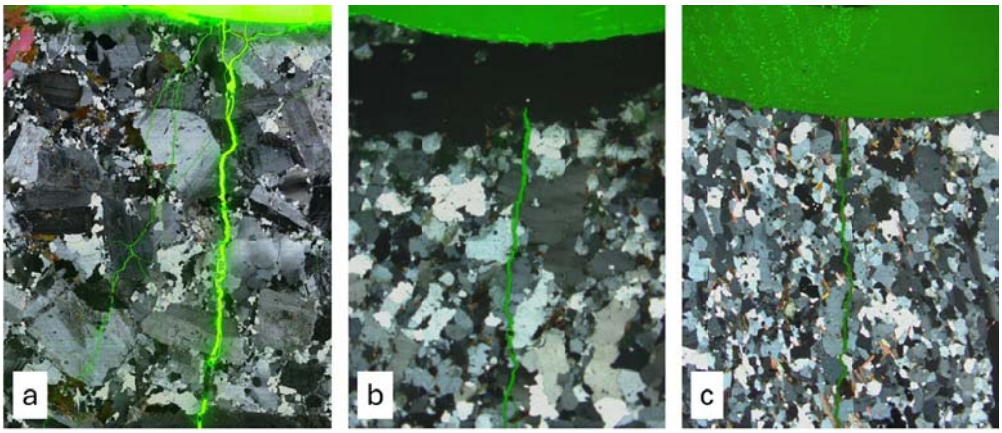


Fig. 9 Thin section images of specimen GR-H3 (a), GN-B1 (b) and GN-C1 (c) in the notch area. Images taken with fluorescent light overlayed on cross polarized light pictures, to enhance the cracks relative the grain structure. Image sizes are 8.4 × 10.8 mm.

4 Discussion and conclusions

The fracture process of one granite and one gneiss was analysed by means of wedge splitting tests and thin sections. The onset of crack initiation was determined based on where stiffness K_{CMOD} versus loading began to deviate from a linear decrease and drop faster during the pre-peak loading phase. The

results complied with determinations done by using strain and displacement fields from DIC measurements. The values of K_{Ic} calculated using non-linear fracture mechanics and LEFM showed a discrepancy. It is noted that the LEFM assumptions are violated e.g. since the rock materials possess a non-linear mechanical behaviour. Moreover, the crack initiation seems to begin before the peak force for the granite. The DIC measurements were further used to visualize the crack propagation, and to quantitatively determine parameters related to the FPZ. The crack branching seen in the granite by the DIC and thin sections is illustrative to understand the more ductile response in the granite and the contrast is large to the gneiss. It was seen that the ligament length was large enough to obtain steady-state crack propagation up to 55–60 mm crack length without influence of the uncracked part (hinge effect). By contrast, often standard LEFM tests are likely not fulfilling this condition which affects the fracture mechanics results which some have pointed out lately. To conclude, some of the used methods are new and some have previously not been fully applied on rock samples and not in a single study. Only a few studies, were the FPZ was examined in rock, were found in the literature. Thin section images confirmed the fracture patterns seen from DIC results and yielded additional detailed results on how the cracks propagated through the microstructures of the two rock types.

5 Acknowledgements

The sampling, sample preparation, experiments and the basic evaluations were carried out within the European project HYDRASPLIT, Grant Agreement No. FP7-SME-2012-1-315530. The advanced evaluations and writing of this paper were partly funded by RISE Research Institutes of Sweden. The use of the figures from other sources complies with the Creative Commons Attribution 4.0 International License.

References

Barenblatt G (1959) The formation of equilibrium cracks during brittle fracture. General ideas and hypotheses. Axially-symmetric cracks. J Appl Math Mech 23(3):622–636. https://doi.org/10.1016/0021-8928(59)90157-1.

Brander L, Flansbjer M, Appelquist K, Casserstedt L, Lindqvist JE(2014) Microtextural fracture study of rock materials subjected to direct tensile tests. CBI Report PX10473, CBI Swedish Cement and Concrete Research Institute, Borås.

Brühwiler E, Wittmann F (1990) The wedge splitting test, a new method of performing stable fracture mechanics tests. Eng Fract Mech 35(1):117–125. https://doi.org/10.1016/0013-7944(90)90189-N.

Jacobsson L, Brander L (2025), Tensile Fracture Initiation and Propagation of Granite and Gneiss at Wedge Splitting Tests: Part 2—Fracturing Studies Based on Digital Image Correlation and Thin Section Analysis. Rock Mech Rock Eng 58, 2031–2054.https://doi.org/10.1007/s00603-024-04257-y.

Jacobsson L, Sandström J, Brander L, Flansbjer M (2025), Tensile fracture initiation and propagation of granite and gneiss at wedge splitting tests: Part—1: Effect of notch type on tensile crack initiation and fracture mechanics results. Int. J. Fracture. https://doi.org/10.1007/s10704-025-00857-z.

Kobayashi T, Fourney WL (1978) Experimental characterization of the development of the micro-crack process zone at a crack tip in rock under load. In: Kim YS (ed) Proc 19th U.S. Symp. Rock Mech., University of Nevada-Reno, May 1978, pp 243–246.

Labuz JF, Shah SP, Dowding CH (1985) Experimental analysis of crack propagation in granite. Int J Rock Mech Min Sci Geomech Abstr 22(2):85–98. https://doi.org/10.1016/0148-9062(85)92330-7.

Labuz JF, Shah SP, Dowding CH (1987) The fracture process zone in granite: evidence and effect. Int J Rock Mech Min Sci Geomech Abstr 24(4):235–246. https://doi.org/10.1016/0148-9062(87)90178-1.

Maji AK, Wang JL (1992) Experimental study of fracture processes in rock. Rock Mech Rock Eng 25(1):25–47. https://doi.org/10.1007/BF01041874.

Sutton MA, Orteu JJ, Schreier H (2009) Image correlation for shape, motion and deformation measurements—basic concepts, theory and applications. Springer. https://doi.org/10.1007/978-0-387-78747-3.

Zhu XK, Joyce JA (2012) Review of fracture toughness (G, K, J, CTOD, CTOA) testing and standardization. Eng Fract Mech 85:1–46. https://doi.org/10.1016/j.engfracmech.2012.02.001.